Geochemical Perspectives Letters

Lanthanum anomalies provide constraints on macrofaunal predation at methane seeps

X. Wang[1,2*], Z. Jia[1], J. Peckmann[3], S. Kiel[4], J.-A. Barrat[5], G. Bayon[6], J. Li[7], L. Yin[8], T. Wei[9], Q. Liang[10], D. Feng[1,2*]

https://doi.org/10.7185/geochemlet.2420

Abstract

The feeding habits and predation behaviour of organisms can exert significant control on the dynamics of local food webs. Yet, little is known about the effects of predation on the material and trophic transfer dynamics in chemosynthesis-based ecosystems. Here, we investigated the rare earth element (REE) composition of soft tissues and hardparts for thiotrophy-dependent vesicomyid clams (*Archivesica marissinica*), aerobic methanotrophy-dependent bathymodiolin mussels (*Gigantidas haimaensis*), in addition to turrid gastropods (*Phymorhynchus buccinoides*) and parasitic scale worms (*Branchipolynoe pettiboneae*) from the Haima seeps of the South China Sea; the latter two species are predators feeding on mussels. Our goal was to determine if the specific, microbially-derived, light REE enrichment characteristics of seep mussels can be transferred to the biomass of their predators. The vesicomyid clams were found to exhibit light REE patterns similar to that of seawater. In contrast, the bathymodiolin mussels, turrid gastropods, and scale worms revealed pronounced lanthanum (La) enrichment, agreeing with substantial transfer of La within the local food web. The observed enrichment of La in seep dwelling predators represents an independent method for monitoring the dynamics within seep ecosystems and potentially for assessing faunal interactions in ancient chemosynthesis-based ecosystems.

Received 23 February 2024 | Accepted 26 April 2024 | Published 28 May 2024

Introduction

Understanding food web structures is essential for comprehending the composition, functionality, and stability of ecosystems. Predation is a crucial component of food web structures and plays a vital role in regulating the population dynamics and maintaining population equilibrium within an ecosystem. Predator–prey interactions also influence species distribution across trophic levels, affecting the flow of energy and matter within the ecosystem. These interactions, in conjunction with adaptation and evolution, contribute to the complexity of food webs and ecological networks. Overall, predator-prey relationships are recognised as important mechanisms in structuring ecosystems (van Denderen *et al.*, 2018).

Submarine seep ecosystems are found worldwide along continental margins (Levin *et al.*, 2016). Unlike ecosystems that rely on photosynthesis, seeps are typified by chemosynthesis-based ecosystems that primarily obtain energy from the oxidation of reduced compounds like methane and hydrogen sulfide. These ecosystems are typified by a low diversity but high abundance of the dominant species (Jørgensen and Boetius, 2007). The community structure is influenced by the availability of energy sources, as well as other factors such as predation, water depth, substrate type, and ecological succession (MacAvoy *et al.*, 2002; Morganti *et al.*, 2022).

The impact of predation on the community structure of seep ecosystems is still not fully understood (Levin *et al.*, 2016). Previous studies have suggested that predators in these ecosystems do not play a dominate role and their influence is typically considered modest (Portail *et al.*, 2016). However, some studies have shown that predation can facilitate trophic transfer and regulate species diversity in seep ecosystems (MacAvoy *et al.*, 2002; Olsen *et al.*, 2014). For example, predation pressure has been found to be the main factor behind the inverse correlation between macrofauna and meiofauna/nematode densities

1. College of Oceanography and Ecological Science, Shanghai Ocean University, Shanghai 201306, China
2. Laboratory for Marine Mineral Resources, Qingdao Marine Science and Technology Center, Qingdao 266237, China
3. Institute for Geology, Center for Earth System Research and Sustainability, Universität Hamburg, 20146 Hamburg, Germany
4. Swedish Museum of Natural History, Department of Palaeobiology, 10405 Stockholm, Sweden
5. Univ Brest, CNRS, Ifremer, IRD, LEMAR, Institut Universitaire Européen de la Mer (IUEM), Place Nicolas Copernic, 29280 Plouzané, France
6. Univ Brest, CNRS, Ifremer, Geo-Ocean, F-29280 Plouzané, France
7. State Key Laboratory of Palaeobiology and Stratigraphy, Nanjing Institute of Geology and Palaeontology and Center for Excellence in Life and Paleoenvironment, Chinese Academy of Sciences, 39 East Beijing Road, Nanjing 210008, China
8. Hebei Key Laboratory of Strategic Critical Mineral Resources, Hebei GEO University, Shijiazhuang 050031, China
9. Department of Ocean Science, The Hong Kong University of Science and Technology, Hong Kong, China
10. MLR Key Laboratory of Marine Mineral Resources, Guangzhou Marine Geological Survey, China Geological Survey, Guangzhou 510070, China

* Corresponding author (email: xd-wang@shou.edu.cn, dfeng@shou.edu.cn)

among the seep benthos (Van Gaever *et al.*, 2009). Predation by metazoans may also explain the differences in copepod abundance between mussel beds and tubeworm colonies at seeps in the Gulf of Mexico (Plum *et al.*, 2015). Moreover, seeps serve as nurseries for deep sea predators, which can greatly affect the diversity of animal species along continental margins (Treude *et al.*, 2011; Danovaro *et al.*, 2022). Understanding the variables influencing the community composition of seep ecosystems, particularly the role of predation, is crucial for comprehending the succession dynamics and the evolution of chemosynthesis-based faunas in Earth history (Treude *et al.*, 2011; Kiel *et al.*, 2016).

Bathymodiolin mussels serve as an ideal focal point for investigating the trophic transfer and the turnover of material within seep ecosystems. Regarding their trophic level, mussels can be classified as primary consumers (Portail *et al.*, 2016). Seep dwelling mussels rely on endosymbiotic primary producers, such as methanotrophic and/or thiotrophic bacteria. In turn, mussels serve as prey for higher level consumers. Representative examples of these higher level consumers include the turrid gastropod *Phymorhynchus buccinoides* and the scale worm *Branchipolynoe pettiboneae* at the Haima seeps of the South China Sea (Fujikura *et al.*, 2009; Takahashi *et al.*, 2012).

Turrid gastropods of the genus *Phymorhynchus* are common in various deep sea habitats such as hydrothermal vents, hydrocarbon seeps, and sunken wood, where they are unspecialised predators that benefit from the high mass of available food in these ecosystems (Sasaki *et al.*, 2010). Stable carbon and nitrogen isotope analysis conducted on *P. buccinoides* specimens collected at the Haima seeps indicated a dependence on local chemosynthetic carbon sources, with the gastropods taking up methane-derived carbon through predation (Ke *et al.*, 2022). *Phymorhynchus* has a well developed, funnel-shaped rhynchostome that facilitates its predatory behaviour (Warén and Bouchet, 2001), and fragments of various organisms in the gut of *Phymorhynchus* have been documented (Sasaki *et al.*, 2010). Its predation on mussels has been demonstrated by *in situ* behavioural observations and bait trap experiments as well as anatomic examination (Fujikura *et al.*, 2009).

Scale worms can thrive in a wide range of habitats and frequently engage in a 'parasitic' relationship with mussels within seep ecosystems (Becker *et al.*, 2013; Yao *et al.*, 2022). Previous stable isotope analyses conducted on scale worms from hydrocarbon seeps indicated their reliance on chemosynthesis-based biomass (Becker *et al.*, 2013; Ke *et al.*, 2022). Based on their jaw structure, it has been inferred that the scale worms exhibit predatory behaviour (Fauchald and Jumars, 1979). Likewise, mussel fragments have been discovered among the stomach contents of the parasitic scale worm *Branchipolynoe symmyitilida* (Desbruyères *et al.*, 1985). Nitrogen stable isotope compositions of amino acids of the scale worm *B. pettiboneae* and its host mussel indicate that the mussel serves as the primary source of amino acids for the adult parasitic worm (Takahashi *et al.*, 2012). Parasitism of *B. pettiboneae* within *G. haimaensis* was confirmed and described in detail by Yao *et al.* (2022).

Here, we developed a new approach to quantify the trophic transfer among seep macrofauna (the thiotrophy-dependent vesicomyid clam *Archivesica marissinica*, the aerobic methanotrophy-dependent bathymodiolin mussel *Gigantidas haimaensis*, the heterotrophic turrid gastropod *P. buccinoides*, and the scale worm *B. pettiboneae*) from the Haima seeps of the South China Sea (Fig. 1, Table S-1), with the latter two species known to be feeding on mussels. We analysed the contents of rare earth elements (REEs), particularly lanthanum (La), of these species to evaluate the predation dynamics in seep ecosystems. This approach is based on the facts that (1) the occurrence of La anomalies in seep dwelling metazoans is a robust fingerprint of methanotrophy since the second step in the aerobic oxidation of methane ($CH_3OH \rightarrow HCHO$) can be catalysed by La (Semrau *et al.*, 2018; Wang *et al.*, 2020), and (2) aerobic methanotrophy-dependent mussels are ubiquitous in seep ecosystems (Wang *et al.*, 2022).

Results

The contents of light REEs in the four examined metazoan species vary from several ng/g to several hundred ng/g. Notably, only two samples of bathymodiolin mussels exhibit contents at the μg/g level (Tables S-2 to S-5). The distribution patterns of REEs in the chemosymbiotic bivalves align with previous studies – the REE compositions of the clams fall between the compositions of terrigenous sediments and seawater, lacking light REE enrichment (Fig. S-2), while the light REE contents in the gills of the mussels are one order of magnitude higher than contents in the clams, particularly with respect to La (Fig. S-3). The scale worms as a whole and some of types of soft tissue (gills and visceral mass) of the turrid gastropods reveal an enrichment of La (Figs. S-4, S-5). However, no such enrichment was observed in the shells of the turrid gastropods (Fig. S-4).

Discussion

By determining the La and Ce anomalies (La/La^* and Ce/Ce^*; Eq. 1 and 2; *cf.* Barrat *et al.*, 2023)

$$La/La^* = La_{sn} \times Nd_{sn}^2/Pr_{sn}^3 \quad \text{Eq. 1}$$

$$Ce/Ce^* = Ce_{sn} \times Nd_{sn}/Pr_{sn}^2 \quad \text{Eq. 2}$$

for four invertebrate species from the Haima seeps, we find that the REE patterns of the thiotrophy-dependent *A. marissinica* resemble the REE compositions of other seep dwelling clams (Wang *et al.*, 2020). Additionally, the La anomaly ($La/La^* = 1.15–2.64$) observed for *A. marissinica* is similar to that of thiotrophy-dependent mussels from seeps on the Costa Rica margin (Barrat *et al.*, 2022a). The Ce anomaly in *A. marissinica* soft tissue ($Ce/Ce^* = 0.23–1.02$) is typically lower than that of its shells ($Ce/Ce^* = 1.08–1.42$). The presence of positive Ce anomalies in shells, agreeing with reducing conditions, is likely indicative of the clams' semi-infaunal lifestyle. In contrast, the shells of the epifaunal mussel *G. haimaensis* yielded minor negative Ce anomalies ($Ce/Ce^* = 0.90–1.03$), reflecting their exposure to oxic seawater. The La anomalies of mussel shells ($La/La^* = 2.10–3.71$) are similar to previous findings ($La/La^* = 2.50–3.92$, Wang *et al.*, 2020) – slightly higher than the La anomalies of *Gigantidas* shells from the Brine Pool and Bush Hill sites of the Gulf of Mexico ($La/La^* = 1.73–2.70$), but significantly lower than the anomalies of two *Bathymodiolus* shells from Edison Seamount ($La/La^* = 7.88–11.89$; Barrat *et al.*, 2022a). While the magnitude of the mussels' La anomaly could possibly relate to the efficiency of La utilisation during aerobic oxidation of methane by their symbiotic bacteria (Lin *et al.*, 2023), understanding the cause of the variability of La enrichment in seep mussels requires further investigation.

Although the observed patterns suggest that aerobic methanotrophy-dependent mussels are typified by a distinctive accumulation of light REEs (Fig. S-3), it appears that these mussels cannot be differentiated from thiotrophy-dependent clams solely based on the extent of the La anomaly. We therefore suggest employing a $(La/Nd)_{sn}$ *vs* $(Pr/Nd)_{sn}$ diagram as a means of differentiation (Fig. 2; *cf.* Wang *et al.*, 2020; Barrat *et al.*, 2022a, 2023). In this diagram, clam soft tissues are primarily situated

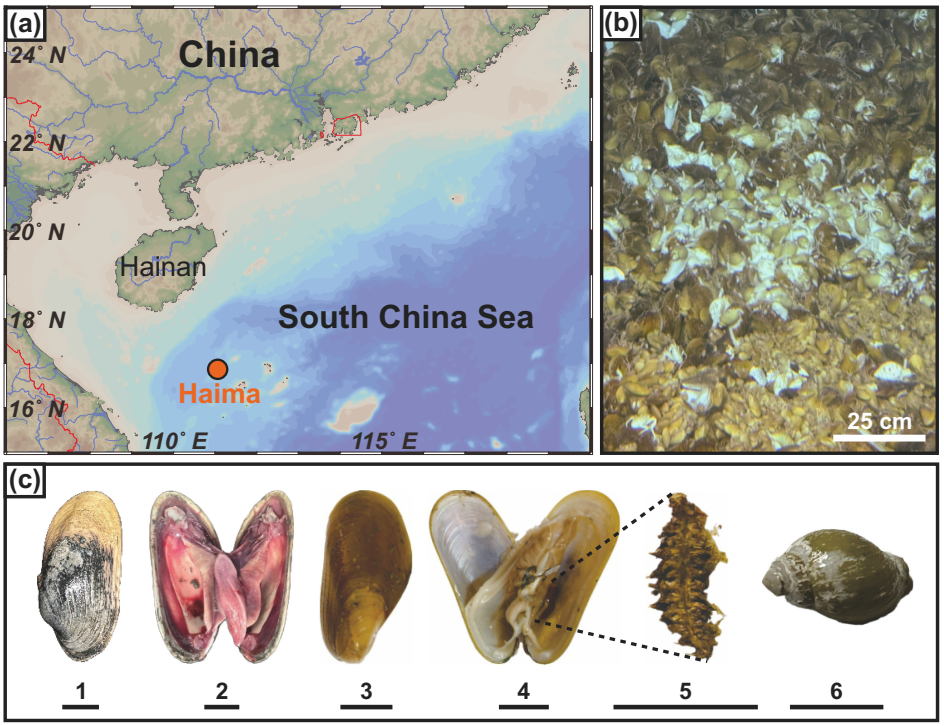

Figure 1 **(a)** Approximate sampling location (Haima seeps). **(b)** Coexisting *Gigantidas haimaensis* (periphery) and *Phymorhynchus buccinoides* (centre) on the seabed. **(c)** Species investigated in this study. **(c1-c2)** *Archivesica marissinica*; **(c3-c4)** *G. haimaensis*; **(c5)** *Branchipolynoe pettiboneae*; **(c6)** *P. buccinoides*. Note that in **c4**, *B. pettiboneae* is parasitic in *G. haimaensis*. Scale bars are 3 cm.

in the lower left corner, with $(La/Nd)_{sn}$ ranging from 0.93 to 2.14 and $(Pr/Nd)_{sn}$ ranging from 0.85 to 1.05. Similarly, clam shells occupy the same region of the diagram, with $(La/Nd)_{sn}$ ratios ranging from 0.99 to 1.22 and $(Pr/Nd)_{sn}$ ratios ranging from 0.84 to 0.91. In contrast, mussel soft tissue – $(La/Nd)_{sn} = 1.25–16.51$, $(Pr/Nd)_{sn} = 0.83–2.22$ – and shells – $(La/Nd)_{sn} = 3.60–8.28$, $(Pr/Nd)_{sn} = 1.20–1.35$ – tend toward the upper right quadrant of the diagram.

With mussels being part of the diet of the predatory gastropod *Phymorhynus* (Fujikura *et al.*, 2009; Sasaki *et al.*, 2010), it is likely that the gastropod assimilates some components of the mussels, and consequently could also acquire the mussels' La enrichment. Indeed, our findings show that the La ($La/La^* = 1.08–3.39$) and Ce anomalies ($Ce/Ce^* = 0.40–1.01$) of *P. buccinoides* closely resemble those of mussels. Predation on mussels is further in accord with the $(La/Nd)_{sn}$ ratios from 1.02 to 3.43, and the $(Pr/Nd)_{sn}$ ratios from 0.88 to 1.14 found in the gills of *P. buccinoides*. The same argument applies to the composition of the gastropod's visceral mass with $(La/Nd)_{sn}$ ratios ranging from 2.86 to 4.05 and $(Pr/Nd)_{sn}$ ratios ranging from 1.04 to 1.25. The shells of *P. buccinoides* ($n = 5$), with $(La/Nd)_{sn}$ ratios ranging from 1.04 to 1.40 and $(Pr/Nd)_{sn}$ ratios ranging from 0.81 to 0.89, do not exhibit significant enrichment of light REEs. Further measurements of additional predatory species with fossilisable hard parts would be needed to test whether this approach can be applied to ancient seep deposits (Kiel *et al.*, 2016).

Scale worms of the genus *Branchipolynoe* are known to parasitise within bathymodiolin mussels (Desbruyères *et al.*, 1985; Becker *et al.*, 2013), and it can therefore be anticipated that they will exhibit positive La anomalies similar to those observed in *P. buccinoides*. Indeed, specimens of *B. pettiboneae* are found to exhibit positive La anomalies ($La/La^* = 2.55–14.23$, $(La/Nd)_{sn} = 2.18–17.42$), likely due to the long term parasitic relationship between the scale worm and mussels, where the scale worm's diet is essentially mussel based. *Phymorhynchus* gastropods, on the other hand, display more omnivorous feeding habits. Interestingly, the degree of the La anomaly in the scale worms is found to be even higher than that of its host mussels (Fig. 2). A potential and simple explanation is that in predator-prey relationships, metal elements become more enriched in organisms of higher trophic levels (biomagnification effect), as in the case of mercury accumulation in the food chain of aquatic organisms (Sun *et al.*, 2020). In summary, *B. pettiboneae* and some of the soft tissues of *P. buccinoides* (gills and visceral mass) exhibit significant enrichment of La. The corresponding La anomalies reflect the interaction between these predatory metazoan species and the aerobic methanotrophy-dependent *G. haimaensis* mussels within the food web structure of the Haima seep ecosystem (Fig. 3).

Finally, we put forward a Bayesian mixing model for assessing the relative contributions of various end members based on the degree of light REE enrichment, with particular focus on the La anomaly. The underlying principle of this method resembles the determination of nutritional interactions among large animals in chemosynthesis-based ecosystems using stable isotopes (Ke *et al.*, 2022). The method is described in detail in the Supplementary Information. In short, the calculation indicates that the proportion of the La anomaly originating from the bathymodiolin mussels – and consequently the food sources – of *P. buccinoides* at the Haima seep site is approximately 50.4 %. This proportion is very similar to the value obtained through the estimate based on stable carbon isotopes (51.0 %; Fig. S-6). When applied to the *B. pettiboneae* from the Haima seep site, the proportion of La anomaly originating from the bathymodiolin mussels is approximately 87.9 %; a proportion almost identical to the value obtained with carbon isotopes (~88.5 %; Fig. S-7). Such estimates suggest that the cycling of La and carbon between tropic levels in seep ecosystems is similar and conservative.

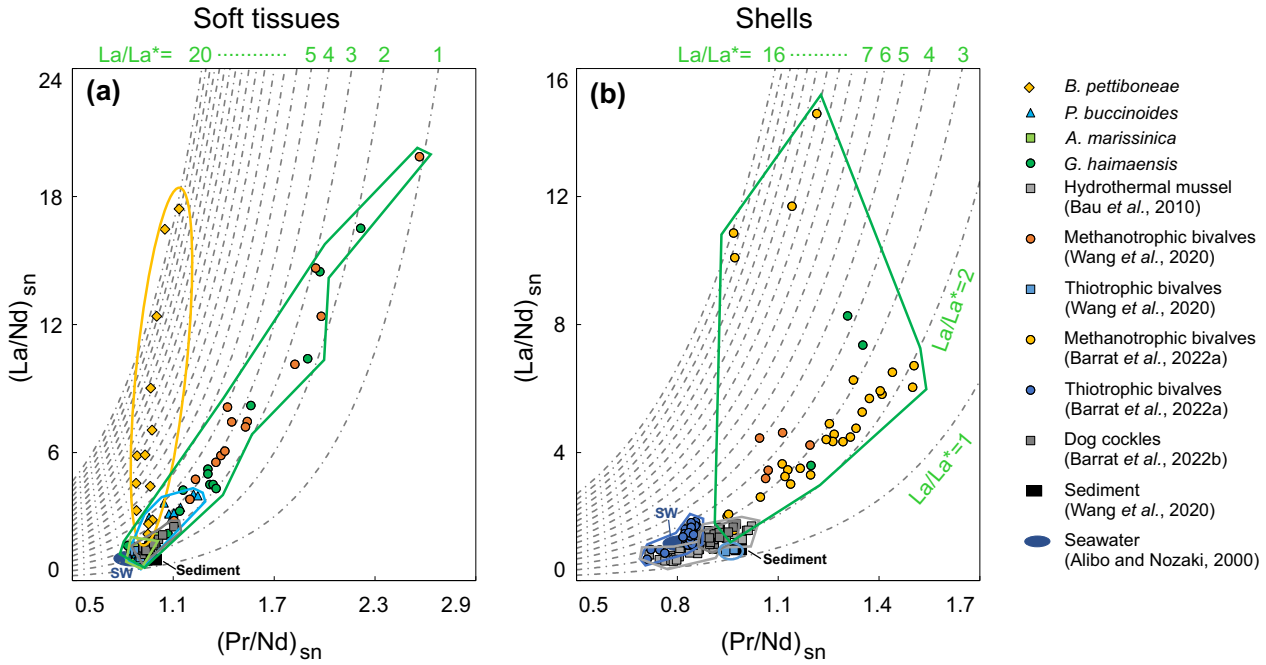

Figure 2 $(La/Nd)_{sn}$ *vs.* $(Pr/Nd)_{sn}$ plots for **(a)** soft tissues and **(b)** shells of various macrofauna from the Haima seeps. Previous work (Bau *et al.*, 2010; Wang *et al.*, 2020; Barrat *et al.*, 2022a,b), seawater (SW; Alibo and Nozaki, 2000) and sediment from the Haima seeps (Wang *et al.*, 2020) are shown for comparison.

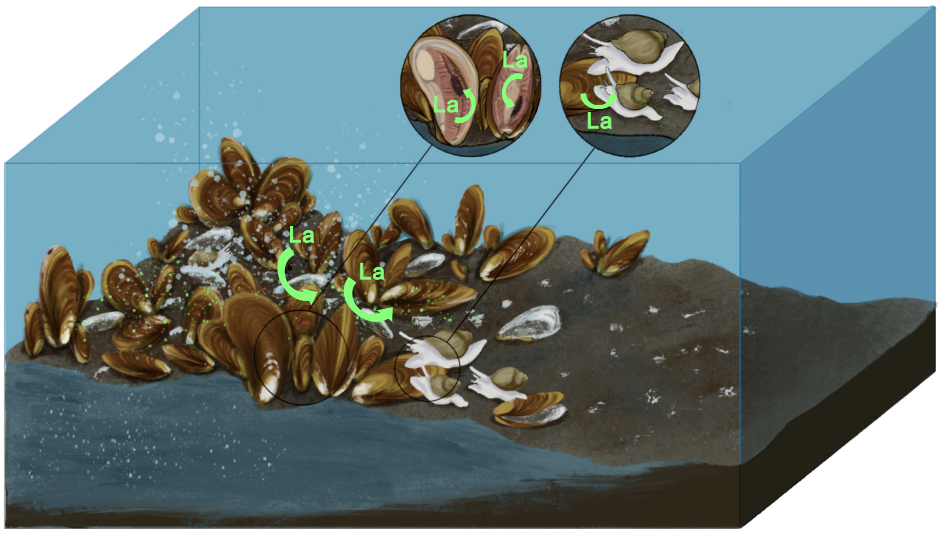

Figure 3 Conceptual diagram of predator-prey interactions within seep ecosystems. La = lanthanum.

Conclusions and Perspectives

Rare earth element (REE) analyses of four invertebrate taxa from the Haima seeps of the South China Sea, the thiotrophy-dependent vesicomyid clam *Archivesica marissinica*, the aerobic methanotrophy-dependent bathymodiolin mussel *Gigantidas haimaensis*, the turrid gastropod *Phymorhynchus buccinoides*, and the scale worm *Branchipolynoe pettiboneae*, revealed that REE compositions faithfully record predation on bathymodiolin mussels by the gastropod and the scale worm. By using a Bayesian mixing model, we have developed a new approach for evaluating the trophic transfer within the food chain at seeps based on REE abundances. Our results suggest that approximately 50 % of the food consumed by the gastropod is sourced from the mussels, whereas mussels could represent up to 90 % to the diet of the scale worm. The novel REE geochemistry approach presented here provides a promising tool for studying the community structure and predator-prey interactions in seep dwelling organisms.

Acknowledgements

Comments provided by editor Andreas Kappler and two anonymous reviewers helped to improve the manuscript. Prof. Jun Tao (Guangzhou Marine Geological Survey, China) is acknowledged for providing the image used in the graphical abstract. We thank the crew of R/V *Haiyang-06* as well as the operation team of *Haima* ROV for their professional assistance throughout the cruises. This study was partially supported by the National

Natural Science Foundation of China (Grants: 42106059 and 42225603), Shanghai Sailing Program (Grant: 21YF1416800) and Chenguang Program of Shanghai Education Development Foundation and Shanghai Municipal Education Commission (Grant: 22CGA58).

Editor: Andreas Kappler

Additional Information

Supplementary Information accompanies this letter at https://www.geochemicalperspectivesletters.org/article2420.

Cite this letter as: Wang, X., Jia, Z., Peckmann, J., Kiel, S., Barrat, J.-A., Bayon, G., Li, J., Yin, L., Wei, T., Liang, Q., Feng, D. (2024) Lanthanum anomalies provide constraints on macrofaunal predation at methane seeps. *Geochem. Persp. Let.* 30, 40–45. https://doi.org/10.7185/geochemlet.2420

References

Alibo, D.S., Nozaki, Y. (2000) Dissolved rare earth elements in the South China Sea: geochemical characterization of the water masses. *Journal of Geophysical Research* 105, 28771–28783. https://doi.org/10.1029/1999JC000283

Barrat, J.-A., Bayon, G., Carney, R.S., Chauvaud, L. (2022a) Rare earth elements as new biogeochemical proxies in deep-sea mussels. *Chemical Geology* 610, 121102. https://doi.org/10.1016/j.chemgeo.2022.121102

Barrat, J.-A., Chauvaud, L., Olivier, F., Poitevin, P., Bayon, G., Salem, D.B. (2022b) Rare earth elements and yttrium in suspension-feeding bivalves (dog cockle, *Glycymeris glycymeris* L.): Accumulation, vital effects and pollution. *Geochimica et Cosmochimica Acta* 339, 12–21. https://doi.org/10.1016/j.gca.2022.10.033

Barrat, J.-A., Bayon, G., Lalonde, T. (2023) Calculation of cerium and lanthanum anomalies in geological and environmental samples. *Chemical Geology* 615, 121202. https://doi.org/10.1016/j.chemgeo.2022.121202

Bau, M., Balan, S., Schmidt, K., Koschinsky, A. (2010) Rare earth elements in mussel shells of the *Mytilidae* family as tracers for hidden and fossil high-temperature hydrothermal systems. *Earth and Planetary Science Letters* 299, 310–316. https://doi.org/10.1016/j.epsl.2010.09.011

Becker, E.L., Cordes, E.E., Macko, S.A., Lee, R.W., Fisher, C.R. (2013) Using stable isotope compositions of animal tissues to infer trophic interactions in Gulf of Mexico lower slope seep communities. *PLoS One* 8, e74459. https://doi.org/10.1371/journal.pone.0074459

Danovaro, R., Fanelli, E., Aguzzi, J., Billett, D., Carugati, L., Corinaldesi, C., Dell'Anno, A., Ggerde, K., Jamieson, A.J., Kark, S., McClain, C., Levin, L., Levin, N., Ramirez-Llodra, E., Ruhl, H., Smith, C.R., Snelgrove, P.V.R., Thomsen, L., Van Dover, C.L., Yasuhara, M. (2022) Ecological variables for developing a global deep-ocean monitoring and conservation strategy. *Nature Ecology & Evolution* 4, 181–192. https://doi.org/10.1038/s41559-019-1091-z

Desbruyères, D., Gaill, F., Laubier, L., Fouquet, Y. (1985) Polychaetous annelids from hydrothermal vent ecosystems: an ecological overview. *Bulletin of the Biological Society of Washington* 6, 103–116.

Fauchald, K., Jumars, P.A. (1979) The diet of worms: a study of polychaete feeding guilds. *Oceanography and Marine Biology Annual Review* 17, 193–284.

Fujikura, K., Sasaki, T., Yamanaka, T., Yoshida, T. (2009) Turrids whelk, *Phymorhynchus buccinoides* feeds on *Bathymodiolus* mussels at a seep site in Sagami Bay, Japan. *Plankton and Benthos Research* 4, 23–30. https://doi.org/10.3800/pbr.4.23

Jørgensen, B.B., Boetius, A. (2007) Feast and famine — microbial life in the deep-sea bed. *Nature Reviews Microbiology* 5, 770–781. https://doi.org/10.1038/nrmicro1745

Ke, Z., Li, R., Chen, Y., Chen, D., Chen, Z., Lian, X., Tan, Y. (2022) A preliminary study of macrofaunal communities and their carbon and nitrogen stable isotopes in the Haima cold seeps, South China Sea. *Deep-Sea Research I* 184, 103774. https://doi.org/10.1016/j.dsr.2022.103774

Kiel, S., Amano, K., Jenkins, R.G. (2016) Predation scar frequencies in chemosymbiotic bivalves at an Oligocene seep deposit and their potential relation to inferred sulfide tolerances. *Palaeogeography, Palaeoclimatology, Palaeoecology* 453, 139–145. https://doi.org/10.1016/j.palaeo.2016.04.026

Levin, L.A., Baco, A.R., Bowden, D.A., Colaco, A., Cordes, E.E., Cunha, M.R., Demopoulos, A.W.J., Gobin, J., Grupe, B.M., Le, J., Metaxas, A., Netburn, A.N., Rouse, G.W., Thurber, A.R., Tunnicliffe, V., Van Dover, C.L., Vanreusel, A., Watling, L. (2016) Hydrothermal vents and methane seeps: rethinking the sphere of influence. *Frontiers in Marine Science* 3, 72. https://doi.org/10.3389/fmars.2016.00072

Lin, Y.-T., Xu, T., Ip, J.C.-H., Sun, Y., Fang, L., Luan, T., Zhang, Y., Qian, P.-Y., Qiu, J.-W. (2023) Interactions among deep-sea mussels and their epibiotic and endosymbiotic chemoautotrophic bacteria: Insights from multi-omics analysis. *Zoological Research* 44, 106–125. https://doi.org/10.24272/j.issn.2095-8137.2022.279

MacAvoy, S.E., Carney, R.S., Fisher, C.R., Macko, S.A. (2002) Use of chemosynthetic biomass by large, mobile, benthic predators in the Gulf of Mexico. *Marine Ecology Progress Series* 225, 65–78. https://doi.org/10.3354/meps225065

Morganti, T.M., Slaby, B.M., de Kluijver, A., Busch, K., Hentschel, U., Middleburg, J.J., Grotheer, H., Mollenhauer, G., Dannheim, J., Rapp, H.T., Purser, A., Boetius, A. (2022) Giant sponge grounds of Central Arctic seamounts are associated with extinct seep life. *Nature Communications* 13, 638. https://doi.org/10.1038/s41467-022-28129-7

Olsen, B.R., Troedsson, C., Hadziavdic, K., Pederson, R.B., Rapp, H.T. (2014) A molecular gut content study of *Themisto abyssorum* (Amphipoda) from Arctic hydrothermal vent and cold seep systems. *Molecular Ecology* 23, 3877–3889. https://doi.org/10.1111/mec.12511

Plum, C., Gollner, S., Martínez-Arbizu, P., Bright, M. (2015) Diversity and composition of the copepod communities associated with megafauna around a cold seep in the Gulf of Mexico with remarks on species biogeography. *Marine Biodiversity* 45, 419–432. https://doi.org/10.1007/s12526-014-0310-8

Portail, M., Olu, K., Dubois, S.F., Escobar-Briones, E., Gelinas, Y., Menot, L., Sarrazin, J. (2016) Food-web complexity in Guaymas Basin hydrothermal vents and cold seeps. *PLoS One* 11, e0162263. https://doi.org/10.1371/journal.pone.0162263

Pourmand, A., Dauphas, N., Ireland, T.J. (2012) A novel extraction chromatography and MC-ICP-MS technique for rapid analysis of REE, Sc and Y: Revising CI-chondrite and Post-Archean Australian Shale (PAAS) abundances. *Chemical Geology* 291, 38–54. https://doi.org/10.1016/j.chemgeo.2011.08.011

Sasaki, T., Warén, A., Kano, Y., Okutani, T., Fujikura, K. (2010) Gastropods from recent hot vents and cold seeps: systematics, diversity and life strategies. In: Kiel, S. (Ed.) *The Vent and Seep Biota*. Springer, Dordrecht, 169–254. https://doi.org/10.1007/978-90-481-9572-5_7

Semrau, J.D., Dispirito, A.A., Gu, W., Yoon, S. (2018) Metals and methanotrophy. *Applied and Environmental Microbiology* 84, e02289–17. https://doi.org/10.1128/AEM.02289-17

Sun, R., Yuan, J., Sonke, J.E., Zhang, Y., Zhang, T., Zheng, W., Chen, S., Meng, M., Chen, J., Liu, Y., Peng, X., Liu, C. (2020) Methylmercury produced in upper oceans accumulates in deep Mariana Trench fauna. *Nature Communications* 11, 3389. https://doi.org/10.1038/s41467-020-17045-3

Takahashi, Y., Sasaki, Y., Chikaraishi, Y., Tsuchiya, M., Watanabe, H., Asahida, T., Maruyama, T., Fujikura, K. (2012) Does the symbiotic scale-worm feed on the host mussel in deep-sea vent fields? *Researches in Organic Geochemistry* 28, 23–26.

Treude, T., Kiel, S., Linke, P., Peckmann, J., Goedert, J.L. (2011) Elasmobranch egg capsules associated with modern and ancient cold seeps: a nursery for marine deep-water predators. *Marine Ecology Progress Series* 437, 175–181. https://doi.org/10.3354/meps09305

van Denderen, P.D., Lindegren, M., MacKenzie, B.R., Watson, R.A., Andersen, K.H. (2018) Global patterns in marine predatory fish. *Nature Ecology & Evolution* 2, 65–70. https://doi.org/10.1038/s41559-017-0388-z

Van Gaever, S., Galeron, J., Sibuet, M., Vanreusel, A. (2009) Deep-sea habitat heterogeneity influence on meiofaunal communities in the Gulf of Guinea. *Deep-Sea Research II* 56, 2259–2269. https://doi.org/10.1016/j.dsr2.2009.04.008

Wang, X., Barrat, J.-A., Bayon, G., Chauvaud, L., Feng, D. (2020) Lanthanum anomalies as fingerprints of methanotrophy. *Geochemical Perspectives Letters* 14, 26–30. https://doi.org/10.7185/geochemlet.2019

Wang, X., Guan, H., Qiu, J.-W., Xu, T., Peckmann, J., Chen, D., Feng, D. (2022) Macro-ecology of cold seeps in the South China Sea. *Geosystems and Geoenvironment* 1, 100081. https://doi.org/10.1016/j.geogeo.2022.100081

Warén, A., Bouchet, P. (2001) Gastropoda and Monoplacophora from hydrothermal vents and seeps; new taxa and records. *The Veliger* 44, 116–231.

Yao, G., Zhang, H., Xiong, P., Jia, H., He, M. (2022) Effects of scale worm parasitism on interactions between the symbiotic gill microbiome and gene regulation in deep sea mussel hosts. *Frontiers in Microbiology* 13, 940766. https://doi.org/10.3389/fmicb.2022.940766

Geochemical Perspectives Letters

Lanthanum anomalies provide constraints on macrofaunal predation at methane seeps

X. Wang, Z. Jia, J. Peckmann, S. Kiel, J.-A. Barrat, G. Bayon, J. Li, L. Yin, T. Wei, Q. Liang, D. Feng

Supplementary Information

The Supplementary Information includes:

- Materials and Methods
- Tables S-1 to S-7
- Figures S-1 to S-7
- Supplementary Information References

Materials and Methods

Sample collection

Four metazoan taxa investigated in this study, including (1) the thiotrophy-dependent clam *Archivesica marissinica*, (2) the methanotrophy-dependent mussel *Gigantidas haimaensis*, (3) the heterotrophic turrid gastropod *Phymorhynchus buccinoides*, and (4) the heterotrophic scale worm *Branchipolynoe pettiboneae* were collected with ROV *Haima* at approximately 1390 m water depth from the Haima methane seeps during a cruise in April 2023 (Fig. 1; Table S-1).

Dissection of macrofauna

The metazoans analysed in this study represent bivalves (one species of clams and mussels each), a gastropod (turrid), and a polychaete (scale worm), all of which possess distinct anatomical structures. To mitigate the risk of metal contamination, a ceramic knife was used for the dissection of metazoans. Clams and mussels were dissected into different types of tissue and hard parts, including adductors, feet, gills, visceral mass, mantle, and shells. Similarly, the turrid gastropod was dissected into columellar muscles, feet, gills, visceral mass, mantle, proboscis, and shells. In order to fulfill the criteria for subsequent geochemical analysis, scale worms were not subjected to dissection due to their limited size and weight (Fig. 1c). The dissected metazoans (and the undissected scale worms) were placed into centrifuge tubes and subjected to freeze-drying in preparation for subsequent analysis.

Rare earth element analysis

Based on the estimation of the rare earth element content in the subsamples, a certain mass of freeze-dried subsample was weighted. The weight of the polychaete as a whole, as well as the soft tissues of bivalves and gastropods, was

approximately 100 mg, while the weight of calcareous shells of bivalves and gastropods was around 200 mg. The samples were then transferred into an acid-washed 7 ml Teflon beaker and soaked in 1 ml concentrated HNO_3. The lid of the Teflon beaker was initially kept open to prevent the accumulation of gas, before the beaker was placed on a heating plate (120 °C). After overnight reaction, the sample was evaporated and 1 ml concentrated HNO_3 was added again to dissolve the sample repeatedly. After two rounds of digestion and evaporation, the samples were subsequently dissolved in a 10 M H_2O_2 (drop by drop until no more bubbles evolved) and evaporated overnight. The samples were finally re-dissolved in a constant volume of 2 ml of 14 N HNO_3 (mother solution).

Due to the low concentration of rare earth elements in the samples and the high concentration of interfering matrix elements, the approach of Barrat *et al.* (2020) and Wang *et al.* (2020) was employed to eliminate the interfering elements (matrix) by passing the mother solution through a DGA resin. The new DGA resin was soaked and rinsed with 0.05 M HCl for 10 times before use. Finally, 1 ml of DGA resin was added to the chromatographic column tube. The detailed procedure was as follows:

Step	**Purpose**	**Operation**
1	Washing matrix elements within DGA resin	5 ml 0.05 N HCl × 10 times
2	Washing matrix elements within DGA resin, maintain acid balance of DGA resin	5 ml 14 N HNO_3 × 1 time
3	Elute all matrix elements (Ca, Mg, Sr) and Ba	3.5 ml 14 N HNO_3 × 2 times
4	Elute Fe	5 ml 2 N HNO_3 × 1 time
5	Collect the target elements (REE + Y)	5 ml 0.05 N HCl × 5 times
Note: Replace the DGA resin after repeating the above operations for 4 times.		

The final step corresponds to the collection of target elements using 25 ml 0.05 N HCl (with a 100 ml plastic bottle, wash it with dilute acid and dry it in advance) followed by evaporation on the hotplate. The re-dissolved sample (in 2 ml 2 % HNO_3, constant volume) with added internal standard was used for analyzing rare earth elements with ICP-MS. The analysis of a standard sample (CAL-S) verified the effectiveness and accuracy of the experimental procedure (Fig. S-1).

Internal standard: 20 ppb Rh
Instrument: Thermofisher iCAPRQ ICP-MS
Standard samples: BHVO-2, W-2a and HPS standard solution (ICP-MS-68A-A-100 and ICP-MS-68A-B-100)
Analytical error: ≤5 %.

Trace element contents of the investigated metazoans are reported on dry matter basis, all rare earth elements were analysed at Hebei GEO University.

The calculation based on the Bayesian mixing model

In this study, we use an open-source R software package, MixSIAR, which is a flexible Bayesian tracer mixing model framework and a customizable tool that was developed on the basis of MixSIR (Moore and Semmens, 2008) and SIAR (Parnell *et al.*, 2010). Readers are recommended to look up the detailed procedures in the original research (Stock *et al.*, 2018).

To validate the Bayesian mixing model, we initially utilised the published carbon isotopes of the investigated metazoans (*i.e.* methanotrophy-dependent mussels, turrid gastropod *Phymorhynchus buccinoides*, and scale worm *Branchipolynoe pettiboneae*) from the Haima seeps. Additionally, we considered the carbon isotopes of dissolved organic carbon (DOC)

and particulate organic carbon (POC) in seawater at the Haima seeps (Table S-7). We employed MixSIAR to simulate the proportion of mussels serving as the carbon source for the turrid gastropod and the scale worm. It is important to acknowledge that the endmembers exhibit slight variation in the simulation of the turrid gastropod and the scale worm, owing to their distinct physiological behavior. The turrid gastropod exhibits a greater degree of omnivorous feeding behavior and has direct contact with sediment, resulting in the utilization of three distinct carbon isotope sources: mussel tissue, DOC, and POC. The scale worm predominantly inhabits methanotrophy-dependent mussels, exhibiting minimal susceptibility to sediments. Consequently, only two endmembers (*i.e.* mussel tissue and DOC), are considered relevant given their ecological niche. The results of the simulation indicate that the proportion of carbon derived from methanotrophy-dependent mussels in the turrid gastropod *Phymorhynchus buccinoides* accounts for approximately 51 % (Fig. S-6 a1 and a2), while in the scale worm *Branchipolynoe pettiboneae*, it accounts for approximately 88.4 % (Fig. S-7 a1 and a2).

Using the La enrichment in metazoan tissue and hard parts ($(La/Nd)_{sn}$) as endmember, the parameters are calculated as follows:

[1] Methanotrophy-dependent mussels:

$$[(La/Nd)_{sn}]_{whole} = \sum([(La/Nd)_{sn}]_F \times mass_F) / \text{total mass} \quad \text{(Eq. S-1)}$$

where F represents adductors, feet, gills, visceral mass, mantle, and shells, respectively. This calculation method implicitly recognises that heterotrophic macrofauna do not exhibit a preference for specific tissues of mussels when preying on them, but rather consume all parts of the mussels in an indiscriminate manner.

[2] Turrid gastropod *Phymorhynchus buccinoides*:
As a heterotrophic omnivorous metazoan, the turrid gastropod has the ability to acquire La from various sources such as seawater, sediments, and mussels. Therefore, the potential sources of La anomalies in their visceral mass are:

$$[(La/Nd)_{sn}]_{visceral\ mass} = F1 \times [(La/Nd)_{sn}]_{SW} + F2 \times [(La/Nd)_{sn}]_{SED} + F3 \times [(La/Nd)_{sn}]_{whole} \quad \text{(Eq. S-2)}$$

where F1, F2 and F3 represent the proportion of $(La/Nd)_{sn}$ from seawater, sediments, and mussels, respectively.

[3] Scale worm *Branchipolynoe pettiboneae*:
Scale worms are unlikely to receive significant contributions of La from sediments. Therefore, the potential sources of La are as follows:

$$[(La/Nd)_{sn}] = F1 \times [(La/Nd)_{sn}]_{SW} + F2 \times [(La/Nd)_{sn}]_{whole} \quad \text{(Eq. S-3)}$$

where F1 and F2 are the proportion of $(La/Nd)_{sn}$ from seawater and mussels, respectively.

[4] Seawater and sediment:
$(La/Nd)_{sn}$ values of seawater and sediment of Haima seeps are taken from the literature (Table S-7).

Using the Bayesian mixing model, it can be calculated that the proportion of La derived from methanotrophy-dependent mussels – and consequently the proportion of mussel tissue among the different food sources – is approximately 50.4 % for the turrid gastropod *Phymorhynchus buccinoides* (Fig. S-6 b1and b2) and approximately 87.9 % for the scale worm *Branchipolynoe pettiboneae* (Fig. S-7 b1 and b2).

Supplementary Tables (Tables S-1 to S-7)

Table S-1 Sample information.

Macrofauna	Species	Trophic mode	Sample ID	Length	Width	Height	Adductors	Feet	Gills	Visceral mass	Mantle	Shells
				(cm)			g (dry weight)					
Bathymodioline mussel	*Gigantidas haimaensis*	Methanotroph	GH1	11.1	5.3	2.2	0.0847	0.1779	0.4519	0.4883	0.5095	5.55
			GH2	11.5	5.4	3.1	0.2776	0.2552	1.4385	1.3075	2.5028	5.75
			GH3	10.2	5.0	2.2	0.2112	0.3681	1.1157	0.6457	0.982	5.1
Pliocardiine clam	*Archivesica marissinica*	Thiotroph	AM1	15.1	6.9	2.5	1.3814	2.2925	6.6673	3.3503	2.2691	—
			AM2	14.7	6.3	2.5	1.1313	1.9154	5.3934	2.2625	1.7688	—
			AM3	15.6	6.7	2.5	1.2684	2.6816	4.9503	3.5415	2.4636	—
				g (as a whole, dry weight)								
Scale worm	*Branchipolynoe pettiboneae*	Heterotroph	BP1	0.0927								
			BP2	0.1522								
			BP3	0.1345								
			BP4	0.1678								
			BP5	0.1422								
			BP6	0.1625								
			BP7	0.1672								
			BP8	0.1535								
			BP9	0.1166								
			BP10	0.0970								
			BP11	0.1434								
			BP12	0.1111								
			BP13	0.1299								
				Columellar muscles			Feet	Gills	Visceral mass	Mantle	Proboscis	Shells
Turrid gastropod	*Phymorhynchus buccinoides*	Heterotroph	PB1	—								
			PB2									

			PB3
			PB4
			PB5

Sampling site: Haima seeps in the northwestern South China Sea
Sampling date: April 2023
Water depth: ~ 1390 m
"—" means no data

Table S-2 ΣREE + Y abundances (in ng/g) of *Archivesica marissinica*.

Sample ID	La	Ce	Pr	Nd	Sm	Eu	Gd	Tb	Dy	Y	Ho	Er	Tm	Yb	Lu	La/La*	Ce/Ce*
Adductors																	
AM1-A	85.59	38.27	11.82	51.12	10.74	2.81	16.21	1.95	9.12	104.86	1.57	3.30	0.37	2.00	0.27	2.28	0.44
AM2-A	162.52	178.72	28.42	112.79	19.89	2.69	12.65	0.51	—	18.73	—	0.78	0.06	0.41	0.07	1.52	0.78
AM3-A	569.10	1068.96	129.70	511.37	100.38	19.67	97.63	9.76	—	326.00	1.12	3.49	0.22	2.08	0.24	1.15	1.02
Feet																	
AM1-F	106.35	54.01	14.05	58.64	11.90	2.99	15.02	1.94	9.32	134.19	1.54	3.22	0.40	2.04	0.29	2.22	0.50
AM2-F	212.65	73.65	28.81	124.82	25.86	6.82	37.90	4.83	24.78	289.81	4.89	11.97	1.33	7.21	1.07	2.33	0.35
AM3-F	202.45	156.21	32.28	132.87	26.96	6.51	33.57	4.33	21.58	242.54	4.25	10.67	1.22	6.69	1.00	1.79	0.62
Gills																	
AM1-G	237.95	51.28	25.89	96.06	13.37	2.73	12.47	0.58	—	51.33	0.33	1.27	0.12	0.87	0.13	2.13	0.23
AM2-G	33.79	33.89	3.80	13.23	2.22	0.46	2.57	0.25	1.02	6.55	0.18	0.48	0.06	0.39	0.06	1.82	0.97
AM3-G	606.31	260.67	82.25	343.02	55.18	6.38	31.72	1.15	—	47.01	—	1.47	—	0.27	0.02	2.16	0.41
Visceral																	
AM1-V	174.38	44.94	20.96	90.99	19.03	4.92	26.07	3.28	16.05	212.84	3.00	6.95	0.80	4.47	0.68	2.64	0.29
AM2-V	239.66	186.06	37.25	156.76	33.55	8.17	39.96	4.44	15.79	278.18	3.80	13.14	1.54	10.55	1.93	1.92	0.66
AM3-V	449.64	432.93	77.70	313.12	62.72	14.29	70.72	8.39	30.01	405.01	3.31	5.46	0.65	3.55	0.46	1.58	0.70
Mantle																	
AM1-M	311.21	99.57	40.04	169.66	35.14	9.07	47.39	6.23	32.69	376.02	6.68	16.63	1.88	9.91	1.53	2.35	0.33
AM2-M	787.65	1186.41	163.85	659.64	133.45	28.47	137.56	18.38	91.32	638.95	17.08	44.19	5.43	31.53	4.53	1.31	0.91
AM3-M	606.37	800.29	122.70	515.17	102.44	22.02	120.64	12.47	43.32	488.05	5.88	13.46	1.48	8.92	1.14	1.47	0.86
Shells																	

AM1-S	4.99	8.88	1.05	4.24	0.94	0.22	1.03	0.14	0.70	4.29	0.13	0.36	0.05	0.31	0.05	1.32	1.08
AM2-S	40.26	65.45	6.31	27.63	5.48	1.26	6.16	0.75	3.74	25.00	0.71	1.86	0.23	1.40	0.21	2.06	1.42
AM3-S	107.22	168.31	16.78	73.69	13.20	3.04	17.07	1.99	10.18	77.19	2.09	5.90	0.72	4.50	0.68	2.08	1.38

"—" means no data

Table S-3 ΣREE + Y abundances (in ng/g) of *Gigantidas haimaensis*.

Sample ID	La	Ce	Pr	Nd	Sm	Eu	Gd	Tb	Dy	Y	Ho	Er	Tm	Yb	Lu	La/La*	Ce/Ce*
Adductors																	
GH1-A	64.38	49.10	4.00	12.72	2.41	0.47	2.26	0.19	0.69	9.15	0.13	0.37	0.05	0.37	0.06	2.73	1.22
GH2-A	74.30	62.26	4.95	13.82	1.49	0.27	1.93	0.13	0.31	12.59	0.04	0.14	0.01	0.08	0.01	1.97	1.10
GH3-A	99.68	134.44	17.07	66.85	13.72	2.79	13.46	1.57	4.89	42.79	0.52	1.06	0.11	0.71	0.10	1.51	0.96
Feet																	
GH1-F	84.85	64.11	4.83	13.62	2.40	0.36	1.84	0.13	0.54	11.05	0.11	0.34	0.05	0.32	0.05	2.35	1.17
GH2-F	87.39	73.64	5.90	16.25	2.31	0.57	3.84	0.38	1.85	23.57	0.39	1.11	0.14	0.87	0.13	1.89	1.07
GH3-F	48.30	43.19	4.59	15.20	2.18	0.48	2.33	0.28	1.16	29.66	0.18	0.50	0.07	0.45	0.08	1.94	0.97
Gills																	
GH1-G	1243.65	363.74	38.58	71.95	11.11	1.87	10.98	0.99	2.68	38.07	0.25	0.49	0.06	0.33	0.04	1.89	0.55
GH2-G	832.58	328.98	34.64	67.08	10.09	1.72	11.51	1.11	4.86	32.87	0.87	2.16	0.26	1.50	0.21	1.52	0.58
GH3-G	1654.08	411.73	50.55	83.91	11.51	2.06	19.61	1.14	2.70	30.64	0.26	0.66	0.05	0.35	0.04	1.52	0.42
Visceral																	
GH1-V	476.61	256.04	20.66	48.66	10.44	1.61	9.33	0.65	1.21	32.30	0.17	0.53	0.06	0.48	0.08	2.16	0.91
GH2-V	192.54	169.81	13.77	37.40	5.18	1.10	6.48	0.73	3.60	28.12	0.70	1.76	0.22	1.23	0.18	1.74	1.05
GH3-V	133.36	133.26	14.72	50.75	10.46	1.91	9.49	0.62	1.81	28.92	0.37	1.23	0.15	1.11	0.20	1.81	0.98
Mantle																	
GH1-M	170.98	131.47	10.17	28.65	4.32	0.76	4.54	0.35	1.15	15.24	0.19	0.51	0.06	0.34	0.05	2.25	1.14
GH2-M	715.76	162.17	82.69	367.13	73.50	18.04	86.44	—	—	463.17	—	1.70	—	1.27	0.08	2.87	0.27
GH3-M	114.50	82.68	9.10	29.44	5.47	1.16	5.68	0.63	2.93	17.38	0.55	1.52	0.19	1.17	0.17	2.21	0.92
Shells																	
GH1-S	52.57	21.00	1.89	5.32	0.93	0.22	1.47	0.14	0.44	12.30	0.06	0.13	0.02	0.10	0.02	3.71	0.98
GH2-S	71.44	36.27	2.99	8.13	1.23	0.44	2.22	0.22	1.06	14.16	0.22	0.60	0.08	0.50	0.08	2.98	1.03
GH3-S	53.54	38.06	4.05	12.45	1.89	0.41	2.90	0.30	1.45	18.26	0.28	0.76	0.10	0.63	0.10	2.10	0.90

"—" means no data

Table S-4 ΣREE + Y abundances (in ng/g) of *Phymorhynchus buccinoides*.

Sample ID	La	Ce	Pr	Nd	Sm	Eu	Gd	Tb	Dy	Y	Ho	Er	Tm	Yb	Lu	La/La*	Ce/Ce*
Columellar																	
PB1-CM	48.10	42.50	6.44	24.26	5.05	0.93	4.41	0.41	0.97	19.42	0.11	0.26	0.03	0.20	0.03	1.79	0.78
PB2-CM	40.15	19.14	3.14	10.75	2.69	0.42	2.38	0.24	0.91	6.88	0.14	0.33	0.04	0.26	0.04	2.53	0.65
PB3-CM	51.87	40.86	5.93	22.22	8.06	1.09	5.91	0.71	3.51	26.69	0.68	1.84	0.24	1.62	0.26	2.07	0.81
PB4-CM	25.98	25.58	3.84	15.06	3.58	0.65	3.27	0.27	0.67	14.77	0.10	0.29	0.04	0.26	0.04	1.76	0.82
PB5-CM	24.23	17.53	3.00	11.69	3.02	0.43	1.97	0.13	0.59	10.73	0.19	0.71	0.08	0.55	0.09	2.07	0.71
Feet																	
PB1-F	457.50	895.60	107.17	415.30	83.30	16.56	80.55	9.32	22.64	278.84	1.66	3.84	0.32	2.45	0.29	1.08	1.01
PB2-F	80.91	139.04	18.40	72.42	15.67	3.01	15.93	1.83	6.39	48.30	0.70	1.40	0.16	0.96	0.11	1.15	0.93
PB3-F	55.53	88.37	10.90	41.64	9.42	1.82	7.95	1.07	5.08	33.92	0.88	2.12	0.28	1.65	0.24	1.25	0.97
PB4-F	37.08	53.16	6.72	26.14	5.59	1.02	4.72	0.46	1.14	20.41	0.12	0.29	0.03	0.23	0.03	1.40	0.96
PB5-F	67.29	102.00	12.18	46.54	13.01	2.02	9.35	1.21	5.64	42.23	0.97	2.41	0.30	1.83	0.26	1.36	1.00
Gills																	
PB1-G	99.09	107.36	17.05	70.18	16.95	3.40	18.01	2.30	11.17	85.32	2.04	5.13	0.66	4.35	0.70	1.66	0.81
PB2-G	333.77	590.77	71.58	274.22	57.38	11.28	53.63	6.51	21.47	171.22	2.32	5.14	0.58	3.83	0.52	1.15	0.99
PB3-G	355.18	245.85	56.93	238.35	47.20	7.69	30.88	—	—	78.98	—	1.27	0.04	0.53	0.05	1.84	0.57
PB4-G	176.93	109.84	13.42	43.21	5.87	0.63	4.78	0.20	—	5.01	—	0.24	0.01	0.07	0.01	2.30	0.82
PB5-G	122.68	55.26	9.04	34.81	9.59	1.48	6.37	0.45	1.15	—	0.18	0.53	0.07	0.36	0.05	3.39	0.74
Visceral mass																	
PB1-V	193.91	124.15	16.74	56.72	6.77	—	4.28	0.22	0.28	1.80	0.07	—	0.04	0.24	0.04	2.24	0.79
PB2-V	348.66	83.47	22.80	80.27	18.09	3.72	22.35	2.48	11.44	124.85	2.07	4.90	0.57	3.40	0.50	3.19	0.40
PB3-V	355.58	228.16	24.38	73.50	12.09	2.48	16.58	1.55	6.15	40.72	0.95	2.15	0.25	1.50	0.20	2.23	0.88
PB4-V	411.81	237.28	29.41	86.81	15.60	3.05	19.82	1.94	8.08	60.71	1.20	2.64	0.33	2.04	0.27	2.06	0.74
PB5-V	175.51	120.73	13.91	46.36	9.70	1.53	8.06	0.39	0.34	—	0.04	—	0.02	0.18	0.02	2.36	0.91
Mantle																	
PB1-M	48.96	62.05	8.71	34.84	7.72	1.51	7.21	0.62	0.91	—	0.08	0.33	0.03	0.25	0.04	1.51	0.89
PB2-M	793.36	1271.11	176.41	688.56	135.03	27.85	125.57	17.30	84.86	535.21	14.27	33.53	4.53	26.33	3.51	1.15	0.88
PB3-M	109.45	178.12	22.76	88.33	19.13	3.62	17.74	2.27	9.02	66.90	1.15	2.24	0.28	1.62	0.20	1.22	0.95
PB4-M	60.87	84.64	10.76	42.28	9.47	1.77	8.87	1.07	4.32	36.99	0.57	1.12	0.14	0.84	0.11	1.47	0.97

PB5-M	41.22	60.24	9.34	36.90	8.62	1.41	6.92	0.83	4.02	22.53	0.85	1.70	0.21	1.31	0.19	1.16	0.80
Proboscis																	
PB1-P	32.63	35.59	5.37	22.18	6.05	1.45	6.95	1.38	16.41	75.58	4.55	11.29	1.35	7.57	1.19	1.74	0.86
PB2-P	19.91	20.85	3.18	12.24	2.90	0.54	2.82	0.33	1.49	9.00	0.26	0.66	0.08	0.52	0.08	1.57	0.79
PB3-P	28.33	23.77	3.58	13.16	3.72	0.58	2.76	0.37	1.85	13.88	0.35	0.92	0.11	0.74	0.12	1.80	0.76
PB4-P	27.29	35.24	5.23	21.77	6.32	1.38	5.74	0.85	5.76	54.71	1.51	4.90	0.59	3.59	0.56	1.52	0.88
PB5-P	24.64	25.20	3.66	13.91	4.22	0.58	2.83	0.30	0.89	—	0.10	0.21	0.02	0.15	0.02	1.64	0.82
Shells																	
PB1-S	114.53	119.09	17.28	72.37	14.11	3.42	15.62	2.11	10.43	95.08	1.76	3.85	0.50	2.84	0.40	1.96	0.90
PB2-S	82.72	88.89	12.70	52.64	11.77	2.73	14.24	1.85	9.10	60.32	1.66	4.30	0.54	3.37	0.49	1.89	0.91
PB3-S	114.60	100.61	20.41	92.40	19.56	5.01	26.98	3.36	15.05	169.42	2.38	5.30	0.65	3.90	0.51	1.94	0.70
PB4-S	124.96	108.12	17.60	74.79	14.37	3.31	15.75	1.78	6.80	86.62	1.00	2.23	0.28	1.68	0.25	2.16	0.82
PB5-S	133.76	144.93	21.75	94.79	19.50	4.70	24.51	3.17	16.46	111.90	3.21	8.25	0.96	5.82	0.83	1.97	0.91

"—" means no data

Table S-5 ΣREE + Y abundances (in ng/g) of *Branchipolynoe pettiboneae*.

Sample	La	Ce	Pr	Nd	Sm	Eu	Gd	Tb	Dy	Y	Ho	Er	Tm	Yb	Lu	La/La*	Ce/Ce*
Whole																	
BP1	239.10	93.21	14.61	60.98	14.17	3.41	20.11	2.46	12.62	113.43	2.66	7.18	0.92	5.60	0.91	4.80	0.83
BP2	536.16	144.29	18.45	76.71	18.02	4.41	23.95	3.05	13.30	167.94	1.90	3.53	0.48	2.64	0.36	8.46	1.02
BP3	416.00	49.71	6.17	20.00	3.73	0.39	2.40	0.14	0.43	2.32	0.09	0.32	0.03	0.20	0.03	11.95	0.82
BP4	314.94	143.91	15.63	59.67	9.90	1.09	7.09	0.47	1.26	12.50	0.28	1.12	0.12	0.74	0.12	4.95	1.10
BP5	328.73	66.97	8.01	30.53	6.93	1.67	8.89	0.99	2.85	58.05	0.39	1.10	0.13	0.85	0.14	10.04	1.00
BP6	344.19	79.98	10.82	40.90	7.31	0.60	3.88	0.18	0.28	4.58	0.08	0.37	0.03	0.19	0.03	7.65	0.87
BP7	125.79	34.69	4.54	17.90	2.01	0.08	1.07	0.08	0.27	—	0.09	0.39	0.05	0.31	0.06	7.27	0.94
BP8	514.47	62.59	7.47	26.17	3.00	0.24	2.98	0.34	1.58	8.18	0.26	0.68	0.10	0.60	0.11	14.23	0.92
BP9	123.73	36.40	5.43	22.73	5.33	1.39	7.33	0.96	3.59	62.36	0.53	1.23	0.17	1.02	0.17	6.74	0.88
BP10	249.54	210.93	24.75	95.94	20.61	4.27	21.17	1.89	3.16	88.73	0.35	1.13	0.12	0.82	0.12	2.55	1.03
BP11	318.65	43.70	5.86	21.54	5.01	1.19	5.37	0.23	0.39	23.10	0.07	0.28	0.04	0.28	0.05	12.37	0.86
BP12	539.66	369.55	42.22	159.13	33.01	6.54	32.89	4.01	15.24	123.03	2.25	5.89	0.73	4.77	0.77	3.06	1.03
BP13	156.00	115.14	12.73	49.21	9.98	1.71	7.49	0.30	0.32	11.55	0.06	0.38	0.03	0.25	0.04	3.08	1.09

"—" means no data

Table S-6 ΣREE + Y abundances (in ng/g) of standard CAL-S in this and previous studies.

Sample ID	La	Ce	Pr	Nd	Sm	Eu	Gd	Tb	Dy	Y	Ho	Er	Tm	Yb	Lu	La/La*	Ce/Ce*
CAL-S																	
This study	603.33	231.24	68.26	286.57	50.64	12.60	74.32	11.48	77.44	1406.37	19.67	60.27	8.11	47.25	7.22	2.62	0.44
Potts *et al.*, 2000	787.00	333.00	90.00	357.00	64.00	16.00	93.00	14.00	100.00	1944.00	26.00	81.00		68.00	11.00	2.32	0.46
Le Goff *et al.*, 2019	793.00	302.00	87.10	359.00	62.40	15.50	91.60	13.70	98.30	2065.00	26.00	81.00		66.30	10.16	2.61	0.45
Wang *et al.*, 2020	806	313	89.2	363	63.7	15.9	92.3	13.9	99.6	2177	26.3	82		67.1	10.3	2.52	0.45
Barrat *et al.*, 2020	806	313	89.2	363	63.7	15.85	92.3	13.9	100	2177	26.33	82		67.1	10.31	2.52	0.45
Barrat *et al.*, 2022	759	310	89.2	369	64.3	16.07	93.3	14	100	2072	26.29	81.9		66.3	10.18	2.45	0.45

Table S-7 Parameters for the Bayesian mixed model.

Sample	$\delta^{13}C$	Reference	Sample	$\delta^{13}C$	Reference
Branchipolynoe pettiboneae	-58.9	Feng *et al.*, 2015	Mussel	-76.4	Feng *et al.*, 2015
	-50.6	Ke *et al.*, 2022		-75.2	
Phymorhynchus buccinoides	-46.9			-73.4	
Phymorhynchus sp.	-48.2			-77.6	
DOC	-22.3	Ding *et al.*, 2022		-76.4	
	-22.4			-72.8	
POC	-28.5	Ke *et al.*, 2022		-74.3	
	-29.7			-69.3	
	-29.5			-67.7	
	-30.6			-70.1	
	-28.2			-69.6	
	-39.3			-65.2	
	-32.4			-71.2	
	-27.2			-68.3	

	-27.2			-64.7	
	-49.8			-70.7	
Mussel	-52.7	Ke *et al.*, 2022		-68.2	
	-60.7	Wang *et al.*, 2022		-66.2	
	-61.9			-71.5	
	-59.8			-68.0	
	-59.3			-66.0	
	-63.7			-70.3	
	-61.7			-69.0	
	-59.8			-66.1	
	-60.8			-72.9	
	-61.8			-72.4	
	-62.8			-68.5	
	-62.9			-74.9	
	-59.3			-73.5	
	-61.5			-69.6	
	-59.3			-70.0	
	-61.0			-68.1	
	-59.0			-66.2	
	-60.0			-71.1	
	-61.3			-70.4	
	-59.3			-66.5	
	-59.9			-63.2	Zhao *et al.*, 2020
	-58.9			-66.6	
	-64.8			-68.7	
	-61.1				
	-58.9		Sample	$(La/Nd)_{sn}$	Reference
	-61.5		Seawater (1488 m, SCS)	1.20	Alibo and Nozaki, 2000
	-63.0		Sediment (Haima)	0.97	Wang *et al.*, 2020

	-60.6	
	-61.8	
	-60.5	
	-61.4	
	-56.3	
	-57.2	
	-55.1	
	-56.2	
	-56.5	
	-52.3	
	-55.2	
	-58.7	
	-53.4	

Supplementary Figures (Figures S-1 to S-7)

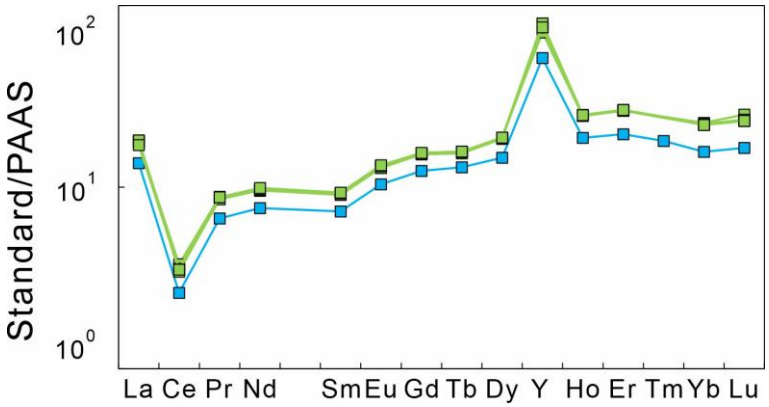

Figure S-1 REE+Y patterns normalised to Post Archaean Australian Shale (PAAS, Pourmand *et al.*, 2012) for the CAL-S standard (blue) analysed during the course of the study. See Table S-6 for the reference values from five other studies (green).

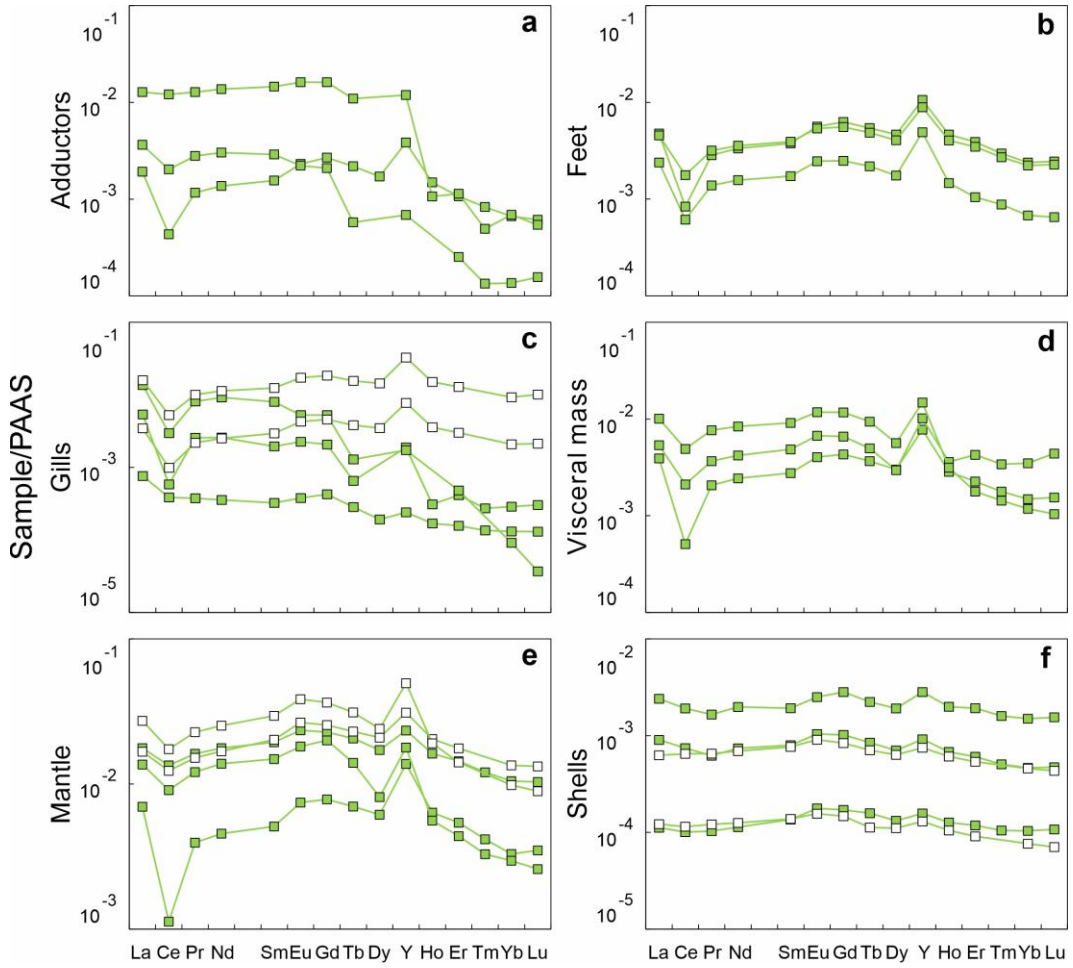

Figure S-2 REE + Y patterns normalised to PAAS (Pourmand *et al.*, 2012) for the clam *Archivesica marissinica* with thiotrophic symbionts from Haima seeps. **(a)** Adductors; **(b)** feet; **(c)** gills; **(d)** visceral mass; **(e)** mantle; **(f)** shells. Data represented by hollow squares are from Wang *et al.* (2020).

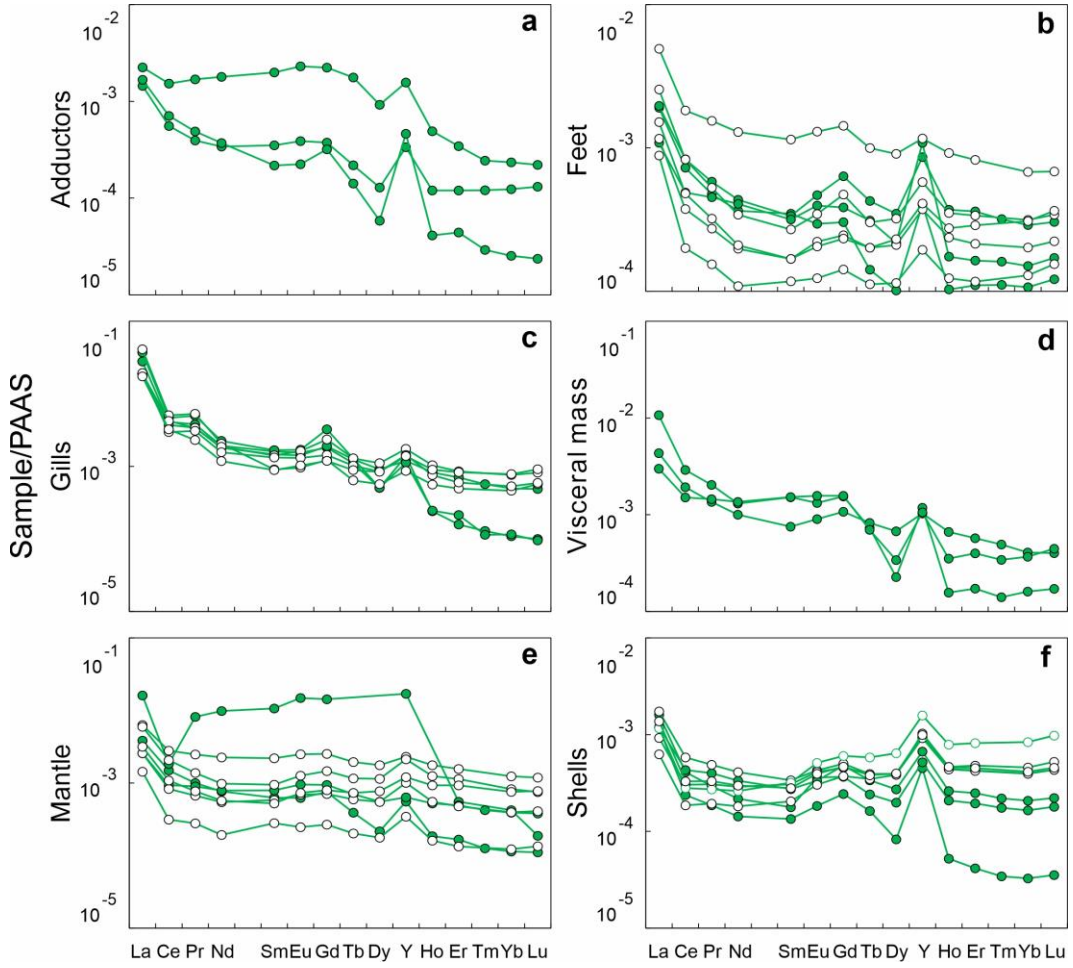

Figure S-3 REE + Y patterns normalised to PAAS (Pourmand *et al.*, 2012) for the mussel *Gigantidas haimaensis* with methanotrophic symbionts from Haima seeps. **(a)** Adductors; **(b)** feet; **(c)** gills; **(d)** visceral mass; **(e)** mantle; **(f)** shells. Data represented by hollow circles are from Wang *et al.* (2020).

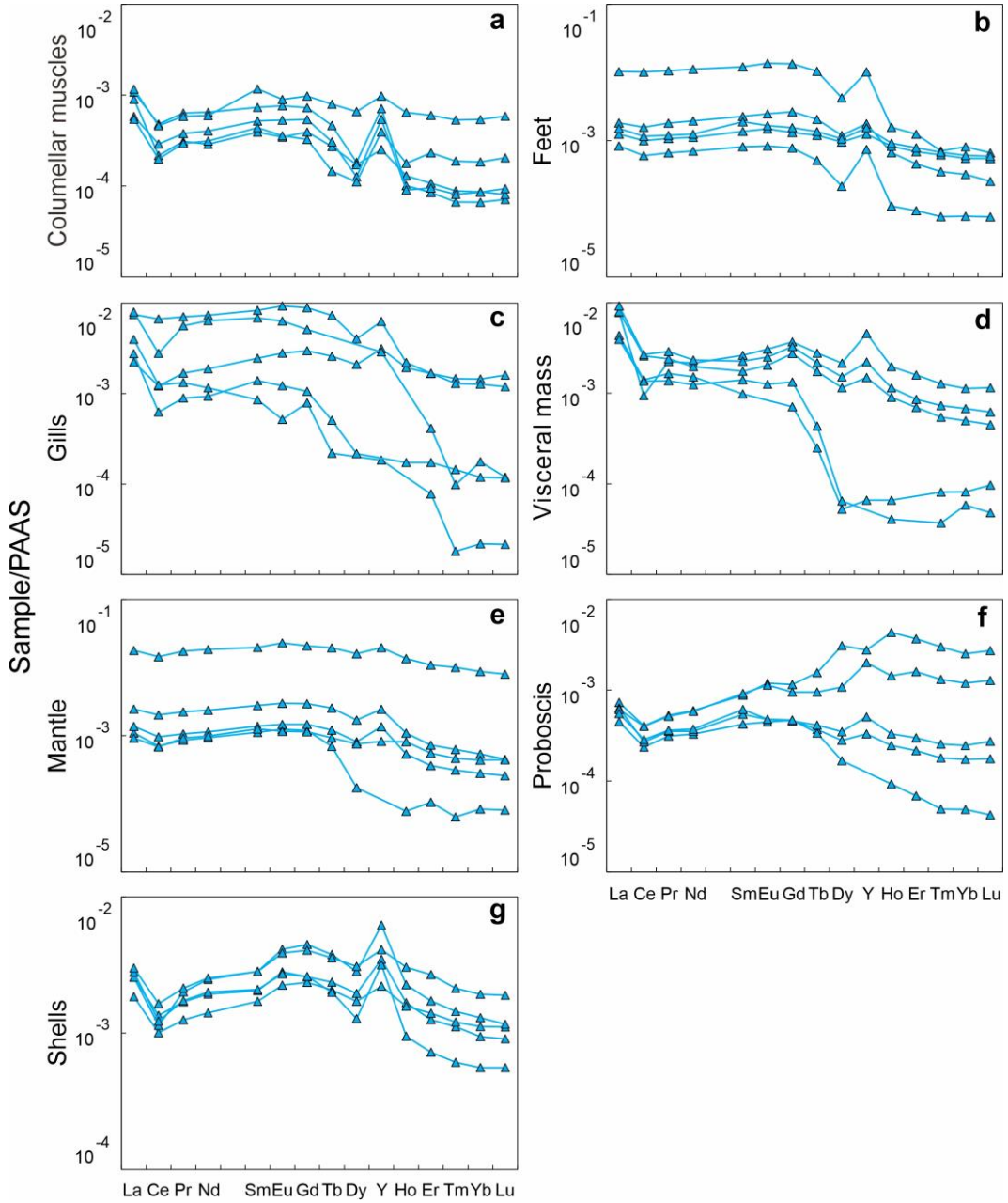

Figure S-4 REE + Y patterns normalised to PAAS (Pourmand *et al.*, 2012) for the heterotrophic turrid gastropod *Phymorhynchus buccinoides* from Haima seeps. **(a)** Columellar muscles; **(b)** feet; **(c)** gills; **(d)** visceral mass; **(e)** mantle; **(f)** proboscis; **(g)** shells.

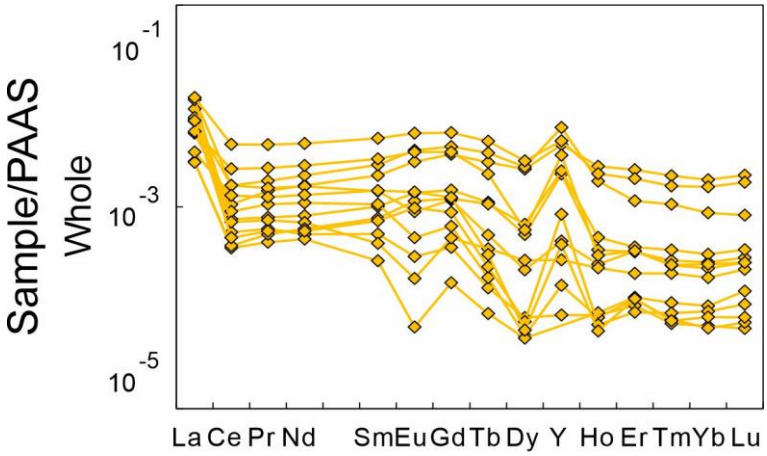

Figure S-5 REE + Y patterns normalised to PAAS (Pourmand *et al.*, 2012) for the heterotrophic scale worm *Branchipolynoe pettiboneae* (as a whole) from Haima seeps.

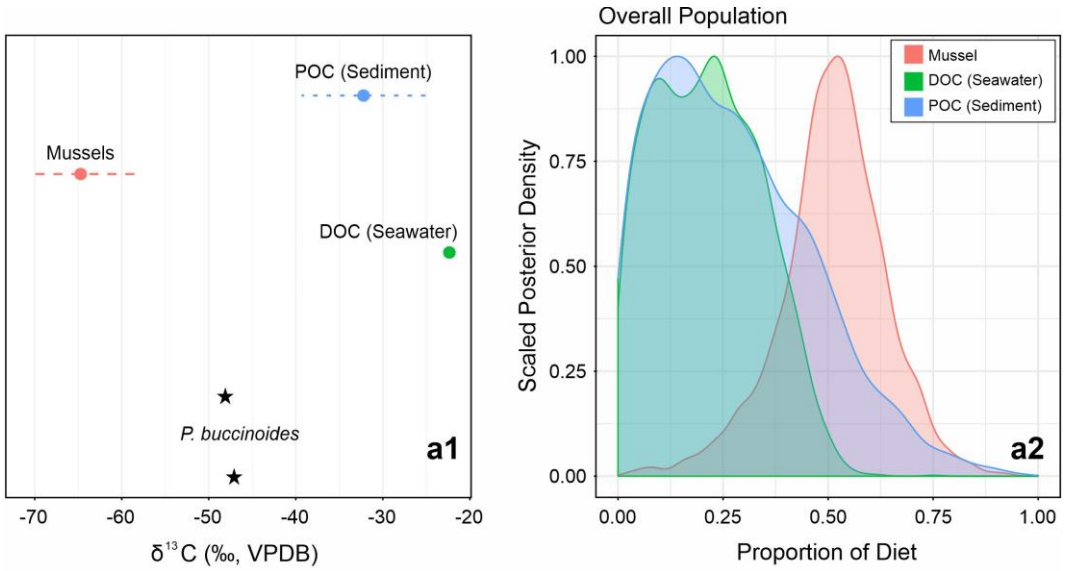

	Mean	SD	2.50 %	5 %	25 %	50 %	75 %	95 %	97.50 %
Mussel	0.510	0.127	0.228	0.286	0.443	0.515	0.589	0.710	0.747
DOC (Seawater)	0.214	0.126	0.011	0.023	0.108	0.209	0.308	0.428	0.460
POC (Sediment)	0.276	0.186	0.012	0.022	0.124	0.251	0.402	0.620	0.691

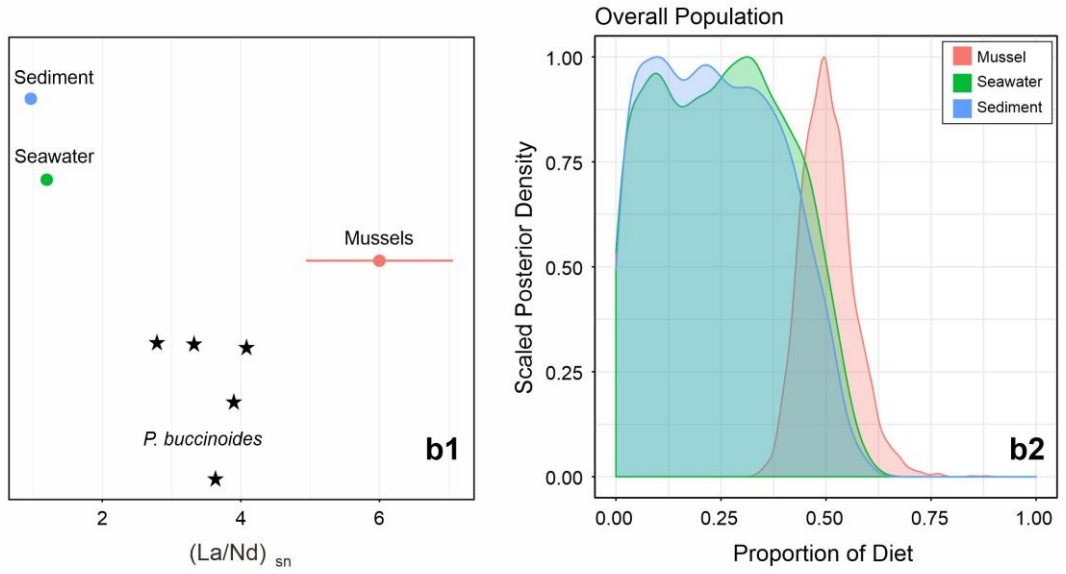

	Mean	SD	2.50 %	5 %	25 %	50 %	75 %	95 %	97.50 %
Mussel	0.504	0.063	0.397	0.412	0.461	0.499	0.54	0.613	0.643
Seawater	0.254	0.152	0.009	0.021	0.121	0.255	0.377	0.499	0.527
Sediment	0.242	0.146	0.013	0.024	0.116	0.235	0.359	0.486	0.513

Figure S-6 Calculation of food sources of the heterotrophic turrid gastropod *Phymorhynchus buccinoides* by a Bayesian mixing model. **(a1-a2)** Based on carbon isotope composition; **(b1-b2)** Based on $(La/Nd)_{sn}$ ratios.

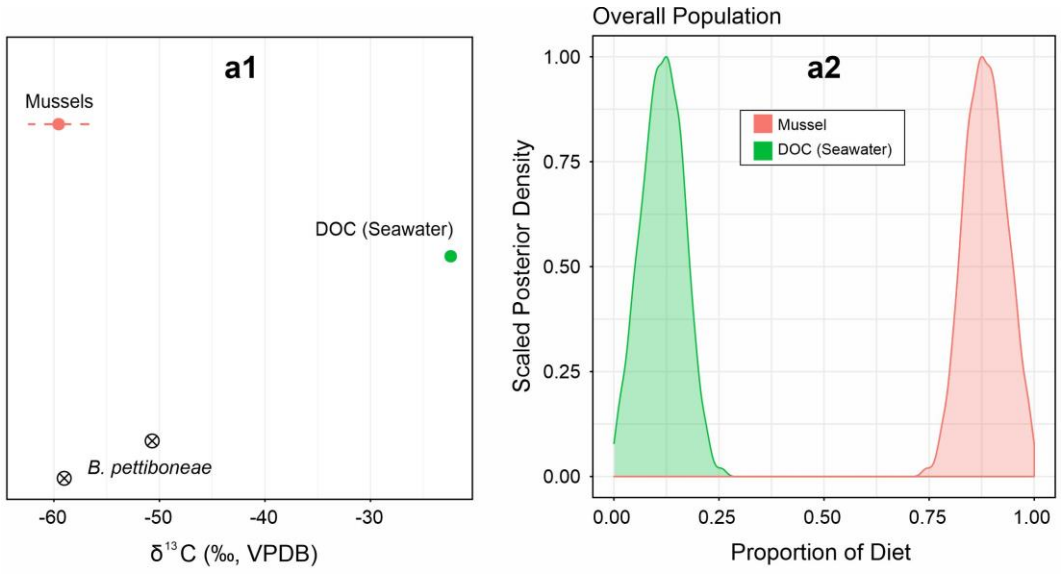

	Mean	SD	2.50 %	5 %	25 %	50 %	75 %	95 %	97.50 %
Mussel	0.884	0.049	0.79	0.805	0.848	0.883	0.919	0.966	0.981
DOC (Seawater)	0.116	0.049	0.019	0.034	0.081	0.117	0.152	0.195	0.21

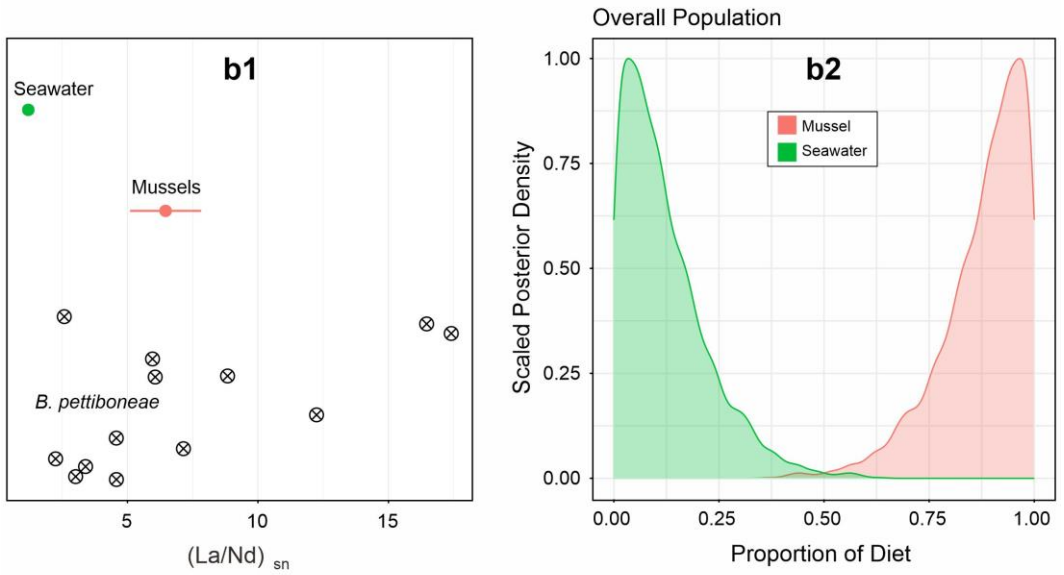

	Mean	SD	2.50 %	5 %	25 %	50 %	75 %	95 %	97.50 %
Mussel	0.879	0.102	0.623	0.68	0.828	0.903	0.957	0.993	0.997
Seawater	0.121	0.102	0.003	0.007	0.043	0.097	0.172	0.32	0.377

Figure S-7 Calculation of food sources of the heterotrophic scale worm *Branchipolynoe pettiboneae* by a Bayesian mixing model. **(a1-a2)** Based on carbon isotope composition; **(b1-b2)** Based on $(La/Nd)_{sn}$ ratios.

Supplementary Information References

Alibo, D.S., Nozaki, Y. (2000) Dissolved rare earth elements in the South China Sea: geochemical characterization of the water masses. *Journal of Geophysical Research* 105, 28771–28783. https://doi.org/10.1029/1999JC000283

Barrat, J.-A., Bayon, G., Wang, X., Le Goff, S., Rouget, M.L., Gueguen, B., Salem, D.B. (2020) A new chemical separation procedure for the determination of rare earth elements and yttrium abundances in carbonates by ICP-MS. *Talanta* 219, 121244. https://doi.org/10.1016/j.talanta.2020.121244

Barrat, J.-A., Chauvaud, L., Olivier, F., Poitevin, P., Bayon, G., Salem, D.B. (2022) Rare earth elements and yttrium in suspension-feeding bivalves (dog cockle, *Glycymeris glycymeris* L.): Accumulation, vital effects and pollution. *Geochimica et Cosmochimica Acta* 339, 12–21. https://doi.org/10.1016/j.gca.2022.10.033

Ding, L., Shan, S., Luo, C., Wang, X. (2022) Distribution and microbial degradation of dissolved organic carbon in the northern South China Sea. *Frontiers in Marine Science* 9, 973694. https://doi.org/10.3389/fmars.2022.973694

Feng, D., Cheng, M., Kiel, S., Qiu, J.-W., Yang, Q., Zhou, H., Peng, Y., Chen, D. (2015) Using *Bathymodiolus* tissue stable carbon, nitrogen and sulfur isotopes to infer biogeochemical process at a cold seep in the South China Sea. *Deep-Sea Research I* 104, 52–59. https://doi.org/10.1016/j.dsr.2015.06.011

Ke, Z., Li, R., Chen, Y., Chen, D., Chen, Z., Lian, X., Tan, Y. (2022) A preliminary study of macrofaunal communities and their carbon and nitrogen stable isotopes in the Haima cold seeps, South China Sea. *Deep-Sea Research I* 184, 103774. https://doi.org/10.1016/j.dsr.2022.103774

Le Goff, S., Barrat, J.-A., Chauvaud, L., Paulet, Y.M., Gueguen, B., Salem, B.D. (2019) Compound-specific recording of gadolinium pollution in coastal waters by great scallops. *Scientific Reports* 9, 8015. https://doi.org/10.1038/s41598-019-44539-y

Moore, J.W., Semmens, B.X. (2008) Incorporating uncertainty and prior information into stable isotope mixing models. *Ecology Letters* 11, 470–480. https://doi.org/10.1111/j.1461-0248.2008.01163.x

Parnell, A.C., Inger, R., Bearhop, S., Jackson, A.L. (2010) Source partitioning using stable isotopes: coping with too much variation. *PLoS One* 5, e9672. https://doi.org/10.1371/journal.pone.0009672

Potts, P.J., Thompson, M., Kane, J.S., Webb, P.C., Carignan, J. (2000) GEOPT6 - an international proficiency test for analytical geochemistry laboratories - report on round 6 (OU-3: Nanhoron microgranite) and 6A (CAL-S: CRPG limestone). International Association of Geoanalysts. https://www.geoanalyst.org/wp-content/uploads/2017/10/GeoPT06-6AReport.pdf

Pourmand, A., Dauphas, N., Ireland, T.J. (2012) A novel extraction chromatography and MC-ICP-MS technique for rapid analysis of REE, Sc and Y: Revising CI-chondrite and Post-Archean Australian Shale (PAAS) abundances. *Chemical Geology* 291, 38–54. https://doi.org/10.1016/j.chemgeo.2011.08.011

Stock, B.C., Jackson, A.L., Ward, E.J., Parnell, A.C., Phillips, D.L., Semmens, B.X. (2018) Analyzing mixing systems using a new generation of Bayesian tracer mixing models. *PeerJ* 6, e5096. https://doi.org/10.7717/peerj.5096

Wang, X., Barrat, J.A., Bayon, G., Chauvaud, L., Feng, D. (2020) Lanthanum anomalies as fingerprints of methanotrophy. *Geochemical Perspectives Letters* 14, 26–30. https://doi.org/10.7185/geochemlet.2019

Wang, X., Guan, H., Qiu, J.-W., Xu, T., Peckmann, J., Chen, D., Feng, D. (2022) Macro-ecology of cold seeps in the South China Sea. *Geosystems and Geoenvironment* 1, 100081. https://doi.org/10.1016/j.geogeo.2022.100081

Zhao, Y., Xu, T., Law, Y.S., Feng, D., Li, N., Xin, R., Wang, H., Ji, F., Zhou, H., Qiu, J.-W. (2020) Ecological characterization of cold-seep epifauna in the South China Sea. *Deep–Sea Research I* 163, 103361. https://doi.org/10.1016/j.dsr.2020.103361